RGNZ/MGPB

Rudarsko-geološko-naftni zbornik
(The Mining-Geology-Petroleum Engineering Bulletin)
DOI: 10.17794/rgn.2026.4.3

Original scientific paper

Numerical Simulation and Regression-Based Prediction of Rotary Disc Cutter Forces in TBM Rock Cutting

Ebrahim Farrokh[1]*, Hamid Rokhy[2], Davood Lotfi[2]
[1] *Amirkabir University of Technology (Tehran Polytechnic), Tehran, Iran.*
[2] *R&D division of Tunnel Saz Machine Co., Tehran, Iran.*

Abstract
This study introduces a computational framework for estimating disc cutter forces during rotary cutting in Tunnel Boring Machines (TBMs), combining LS-DYNA with a Smoothed Particle Galerkin (SPG) approach and the Riedel–Hiermaier–Thoma (RHT) material model. A total of 58 simulations were performed to examine how cutter forces vary with radial installation position, rock strength, contact area, and cutter spacing. The results demonstrate that normal, rolling, and side forces increase with rock compressive strength and contact interface size, but decrease as the cutter's installation radius grows. Regression analysis based on natural logarithmic transformations yielded predictive equations with high accuracy (R^2 = 0.80–0.91). Each fitted parameter is reported with its standard error and 95% confidence interval, ensuring transparency, reproducibility, and statistical robustness.

Keywords:
Rotary disc cutting; SPG; RHT; Cutter force prediction; Regression-based modelling

1. Introduction

Tunnel Boring Machines (TBMs) play a critical role in contemporary underground construction, especially in hard rock environments where accurate prediction of cutter forces is vital for optimizing machine performance and cutterhead design. The forces acting on disc cutters – normal, rolling, and side – vary significantly across the cutterhead zones (centre, face, and gage), and their precise estimation directly impacts operational efficiency. Predicting TBM performance and advance rates in hard rock conditions remains a significant challenge in tunnelling engineering. Recent empirical and machine-learning approaches have focused on developing models for TBM advance rate prediction and geotechnical risk assessment using field data and geological parameters (**Arbabsiar et al., 2020a, 2020b**). While these models provide valuable insight into overall TBM performance metrics, they do not address the fundamental mechanics of individual cutter forces at specific radial positions on the cutterhead – a critical gap for detailed cutterhead design optimization.

Traditionally, key design parameters such as cutter spacing and penetration rate have been derived from large-scale linear cutting tests, which are instrumental in elucidating rock cutting dynamics. These tests offer valuable insight into the interaction between rock and cutting tools, enabling performance optimisation across diverse geological conditions (**Entacher & Lassnig, 2012; Farrokh et al., 2015; Thyagarajan & Rostami, 2024; Pan et al., 2021**). However, linear tests fail to replicate the rotary motion of actual TBM cutterheads, where circular trajectories influence chip formation and force distribution – introducing limitations when extrapolating linear test results to rotary cutting scenarios.

Although rotary cutting experiments have been conducted, they remain limited and often differ markedly from field conditions. For instance, the continuous rotary cutting tests by **Geng et al. (2017, 2024)** differ fundamentally from real-world operations. Recent studies (**Deng et al., 2024; Huang et al., 2024; Zhang et al., 2024; Palassi et al., 2025**) confirm that cutter forces vary with rotation radius, yet comprehensive predictive models that account for radial position remain underdeveloped.

Given the high cost and complexity of physical testing, numerical modelling has emerged as a powerful tool for investigating rock-cutter interactions. The Finite Element Method (FEM) is particularly favored for its ability to accommodate material heterogeneity, nonlinearity, and complex boundary conditions (**Jaime, 2011; Yu, 2005**). Advanced three-dimensional FEM models have successfully simulated complete cutting processes, including crack initiation, propagation, and chip forma-

* Corresponding author: Ebrahim Farrokh
e-mail address: e.farrokh@aut.ac.ir
Received: 20 October 2025. Accepted: 14 January 2026.
Available online: 21 July 2026

tion, with cutting force deviations as low as 7–11% compared to laboratory results (**Jaime, 2011; Khosravi et al., 2021**). Understanding rock fracture mechanisms under dynamic loading is crucial for accurate cutting simulations, with recent discrete element modelling demonstrating the importance of discontinuities and micro-parameters in controlling fracture patterns and strength properties (**Hajibagherpour et al., 2020; Aftabi & Ahangari, 2023**). These models facilitate parametric studies on factors such as cutting speed, bit geometry, confining stress, and pore pressure (**Yu, 2005; Tulu, 2009**), offering valuable insight for improving drilling performance and equipment design while minimizing reliance on costly experiments. Nonetheless, many existing approaches simplify the cutting problem into two-dimensional indentation models or fail to capture the full dynamics of three-dimensional rotary cutting. One note to consider is that in underground excavation environments, in-situ stress conditions significantly affect rock failure behaviour (**Moomivand et al., 2022**), though the present study focuses specifically on intact rock cutting under controlled conditions to establish fundamental force relationships.

Recent advancements in 3D dynamic simulations have further enhanced TBM disc cutting analysis. **Wang et al. (2010)** utilized ANSYS/LS-DYNA to simulate dual disc cutters cutting soft rock, examining phase angle effects and stress field distributions. These specialized platforms enable detailed modelling of fracture propagation and material failure under dynamic loading. **Xu et al. (2022)** validated discrete element models against full-scale linear cutting tests, demonstrating effective estimation of specific energy. **Tan et al. (2013)** contributed by developing 3D FEM models in Abaqus to simulate cutter kinematics during wear, incorporating failure mechanisms and achieving experimental verification.

Mesh-free methods, particularly Smoothed Particle Hydrodynamics (SPH), have shown promise in modelling large deformations during cutting. **Jeong et al. (2013)** applied SPH in AUTODYN-3D to simulate TBM disc cutter rock interaction, achieving cutting force predictions within 10% of experimental values and accurately determining optimal cutter spacing. Traditional Lagrangian methods often suffer from element distortion and reliance on erosion-based approaches, which compromise accuracy under large deformation. Mesh-free algorithms like SPH and Smoothed Particle Galerkin (SPG) improve stability and realism by avoiding erosion dependence. Discrete element methods, such as particle flow code, have also been effective in simulating rock fragmentation, with validation against linear cutting tests on Colorado red granite showing strong correlation in cutting coefficients and specific energy estimates (**Xu et al., 2022**).

Despite these advances, no existing numerical framework provides force estimation formulas that incorporate radial cutter position across all cutterhead zones. Industry models such as the CSM model (**Schlicke et al., 2024; Ko et al., 2014; Rostami, 1997**) and field-based approaches (**Farrokh, 2022; Salimi et al., 2022; Armaghani et al., 2021**) continue to rely on linear cutting data, overlooking the complexities of rotary cutting.

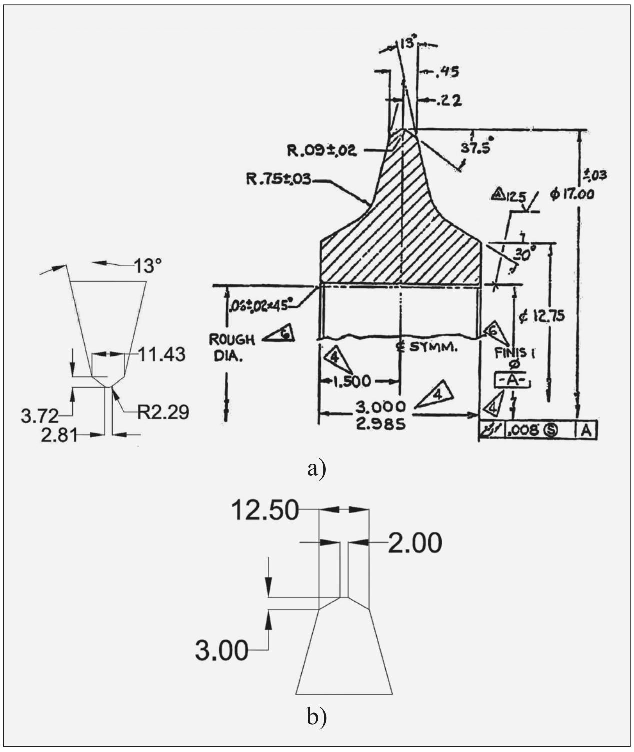

Figure 1: Cross-sectional geometries of the disc cutters used in the simulations: (a) 17-inch disc profile based on Colorado red granite cutting tests (**Rostami, 1997**); (b) 12-inch disc tip design from Tunnel Saz Machine Co. All dimensions are presented in millimetres.

To address this gap, Tunnel Saz Machine Co. initiated the development of a rotary cutting simulation framework using LS-DYNA, integrating the SPG mesh-free algorithm with the RHT material model. This hybrid approach applies SPG to the disc–rock interaction zone and Lagrangian elements to the bulk rock volume, balancing computational efficiency with modelling accuracy. Focusing on intact rock, the study aims to derive regression-based formulas for predicting normal, rolling, and side forces as functions of radial position, contact area, and rock strength. Unlike existing empirical models that focus primarily on advance rate prediction and overall TBM performance assessment (**Arbabsiar et al., 2020a; Zhou et al., 2023**), this research provides detailed force predictions for individual cutters at specific radial locations, enabling more precise cutterhead design optimisation and cutter layout planning. These findings offer a novel pathway for enhancing TBM cutterhead design and performance forecasting in rotary cutting environments. It is important to note that the simulation framework adopted here – including the SPG domain configuration, RHT material parameters, and

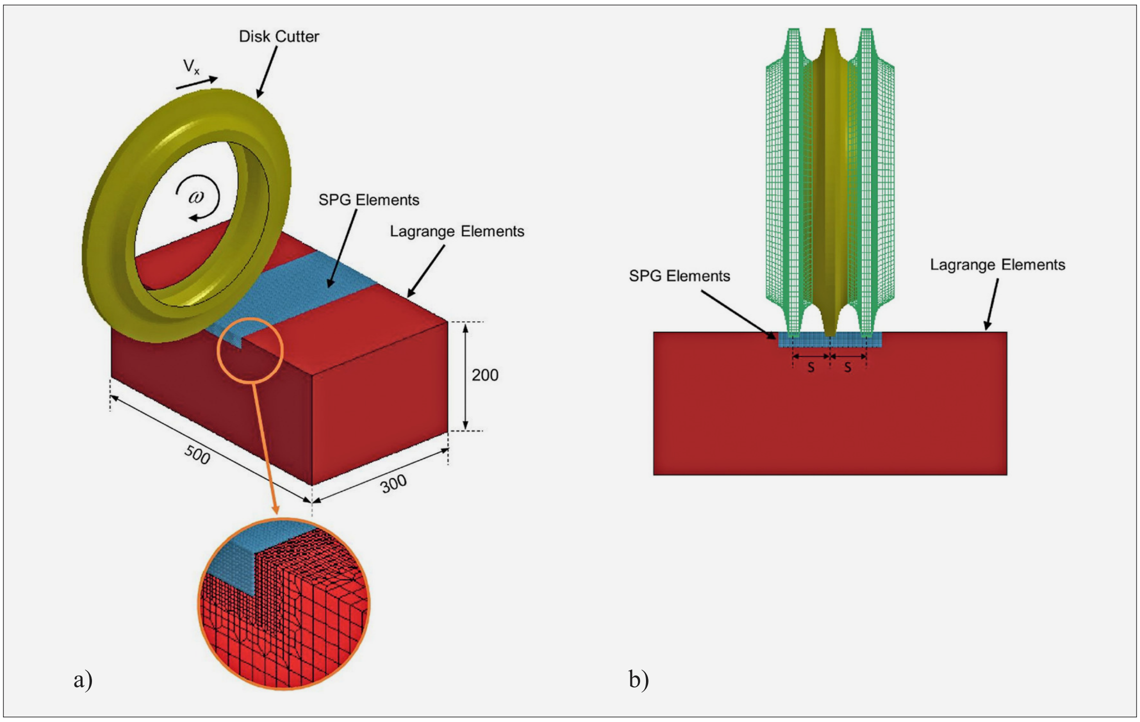

Figure 2: Configuration of the LS-DYNA rotary cutting simulation model: (a) three-dimensional view showing the cutter disc and rock block with dimensions in millimetres; (b) front view illustrating the targeted application of the SPG algorithm in the disc–rock interaction zone.

LS-DYNA strategy – builds directly upon the validated modelling approach presented by **Farrokh et al.** (**2024a, 2024b**), which demonstrated strong agreement with experimental cutting tests on Colorado red granite. As such, the current study extends a previously benchmarked setup to a broader parametric space, ensuring the reliability and applicability of the presented regression models.

2. Numerical modelling

2.1. Disc profiles

The numerical analyses incorporated two distinct disc cutter geometries to reflect real-world cutting conditions. The first profile corresponds to a 17-inch disc (model A30581), previously utilized in linear cutting experiments on Colorado red granite at the Colorado School of Mines (**Rostami, 1997**). The second profile represents the tip geometry of a 12-inch disc developed by Tunnel Saz Machine Co., designed for rotary cutting applications. The cross-sectional geometries of both discs, with dimensions given in millimetres, are shown in **Figure 1.** These geometries were selected to capture the influence of cutter size and tip configuration on force generation during rotary interaction with rock.

2.2. Computational method

The LS-DYNA platform offers several computational strategies for simulating dynamic interactions, including the Lagrange method, Smoothed Particle Hydrodynamics (SPH), and Smoothed Particle Galerkin (SPG). Each approach has distinct advantages depending on the deformation scale and complexity of the modelled process.

- The Lagrangian method, while widely used in finite element analysis, can yield inaccurate results in high-deformation scenarios due to its reliance on erosion-based element deletion. This limitation affects the fidelity of rock-cutting simulations, where material failure and fragmentation are critical.
- SPH, introduced in the late 1970s, replaces traditional mesh structures with discrete particles, enabling effective modelling of large deformations and irregular geometries. However, SPH demands substantial computational resources and poses challenges in defining boundary conditions.
- SPG builds upon SPH by incorporating Galerkin formulations, enhancing numerical stability – particularly under tensile loading – and improving accuracy in simulating brittle material behaviour. Recent applications of SPH and SPG in rock mechanics have demonstrated their effectiveness in capturing complex fracture processes (**Jeong et al., 2020; Wicaksana et al., 2021**).

Farrokh et al. (2024b) showed that mesh-free methods like SPH and SPG outperform erosion-dependent Lagrangian models in simulating rock cutting. Their study revealed a 100% variation in cutting force predictions when the erosion threshold was adjusted from 0.1 to 0.15 in Lagrange-based simulations of Colorado red granite.

Considering these factors, the SPG algorithm was selected for modelling the disc–rock interaction zone, where accurate force prediction is essential. To balance precision with computational efficiency, a hybrid configuration was adopted: Lagrange elements were used for the bulk rock volume, while SPG particles were applied to the region directly influenced by the cutter – defined as three times the penetration depth and three times the cutter spacing in width.

The final simulation setup, highlighting the targeted use of SPG in critical zones to enhance modelling accuracy without incurring excessive computational cost, is shown in **Figure 2**.

2.3. Constitutive material model

To simulate the mechanical behaviour of rock under dynamic cutting conditions, the Riedel-Hiermaier-Thoma (RHT) model was selected within LS-DYNA. This advanced plasticity-based damage model is specifically designed for brittle materials such as concrete and rock (**Riedel et al., 2009**). It incorporates three distinct strength surfaces – yield, failure, and residual – that collectively describe the material's response from initial loading through complete degradation.

- Yield Surface: Marks the onset of plastic deformation, constrained by a cap to ensure volumetric consistency.
- Failure Surface: Defines the threshold at which damage begins to accumulate.
- Residual Surface: Represents the fully degraded state, where strength is governed by residual parameters.

The model also accounts for strain rate sensitivity, enabling accurate simulation of dynamic loading scenarios (**Tu and Lu, 2009**). The elastic limit surface is scaled from the failure surface using a pressure-dependent factor and a parabolic cap function, as shown in **Figure 3** (**Tu and Lu, 2009; Riedel et al., 2009**). The post-failure behaviour is modelled using a damage factor D, which interpolates between the failure and residual surfaces (**Chen, 1982**).

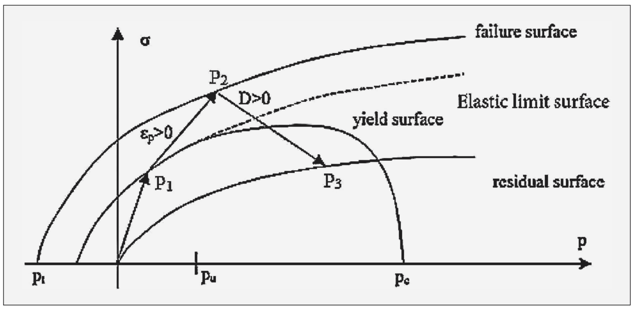

Figure 3: Representation of the RHT model's strength surfaces – yield, failure, and residual – illustrating the material's progressive response under loading and damage accumulation (adapted from **Tu and Lu, 2009**).

Table 1: Input parameters for the Riedel-Hiermaier-Thoma (RHT) material model used to simulate Colorado red granite behaviour in LS-DYNA, adapted from **Xie et al. (2017)**

Parameter	Value	Parameter	Value
Density (kg/m^3)	2660	NP	3.0
ALPHA	0	EOC	3E-5
PEL (MPa)	125	EOT	3E-6
PCO (GPa)	6.0	EC	3E+25
A_1 (GPa)	25.7	ET	3E+25
A_2 (GPa)	37.84	BETAC*	0.026
A_3 (GPa)	21.29	BETAT**	0.007
B_0	1.22	PTF	0.001
B_1	1.22	GC*	0.53
T_1 (GPa)	25.7	GT*	0.7
T_2	0.0	EPSF	2.0
SHEAR (GPa)	21.9	XI	0.5
FC (MPa)	158	D_1	0.04
FT	0.04	D_2	1.0
FS	0.21	EPM	0.015
A	2.44	AF	0.25
N	0.76	AN	0.62
Q0	0.68	GAMMA	0.0
B	0.05		

* Exponent for compressive strain rate sensitivity
** Exponent for tensile strain rate sensitivity

For this study, material parameters for Colorado red granite were adopted from **Xie et al. (2017)**, as summarized in **Table 1**. These values enable accurate representation of the rock's strength and deformation characteristics under rotary cutting loads.

3. Numerical analysis plan for the rotary cutting tests

To investigate the mechanical response of disc cutters under rotary cutting conditions, a comprehensive simulation matrix was developed. The analyses focused on key parameters known to influence cutter forces, including rock strength, cutter geometry, penetration depth, spacing, and radial installation position.

The rock's uniaxial compressive strength (UCS) was varied across four representative values: 50, 70, 115, and 158 MPa. Two disc diameters – 17 inches and 12 inches – were selected based on industry-standard configurations (see **Figure 1**). Cutter tip widths of 12.5 mm and 20 mm were included to assess contact mechanics. Penetration depths ranged from 4 to 12 mm, while cutter spacing was set at 25, 51, and 76 mm. Radial positions on the cutterhead were modelled at 250, 500, and 1000 mm to capture zone-specific force variations.

The simulations computed three primary force components acting on the disc cutter: normal force (Fn), roll-

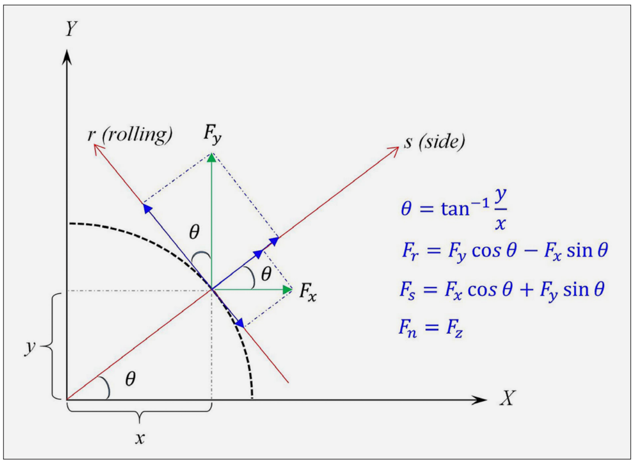

Figure 4: Force component calculation in rotary cutting simulations: transformation between the global coordinate system (X, Y, Z) and the disc-attached local system (r, s, n), with the dashed curve representing the cutter's rotational path

ing force (Fr), and side force (Fs). These were derived by resolving the interaction forces between the disc and rock within two coordinate systems: a fixed global frame (X, Y, Z) and a rotating local frame attached to the disc (r, s, n). The transformation between these systems, with the dashed curve representing the cutter's trajectory and the Z/n axes oriented perpendicular to the cutting plane, is shown in **Figure 4.**

3.1. Results of numerical analyses

The rotary cutting simulations produced detailed force data across a wide range of input conditions. Each analysis yielded values for normal force (Fn), rolling force (Fr), and side force (Fs), corresponding to specific combinations of cutter geometry, penetration depth, spacing, radial position, and rock strength.

To quantify the contact interface between the disc and rock, the contact area (Acon) was calculated using a graphical method. This involved analysing cutter inden-

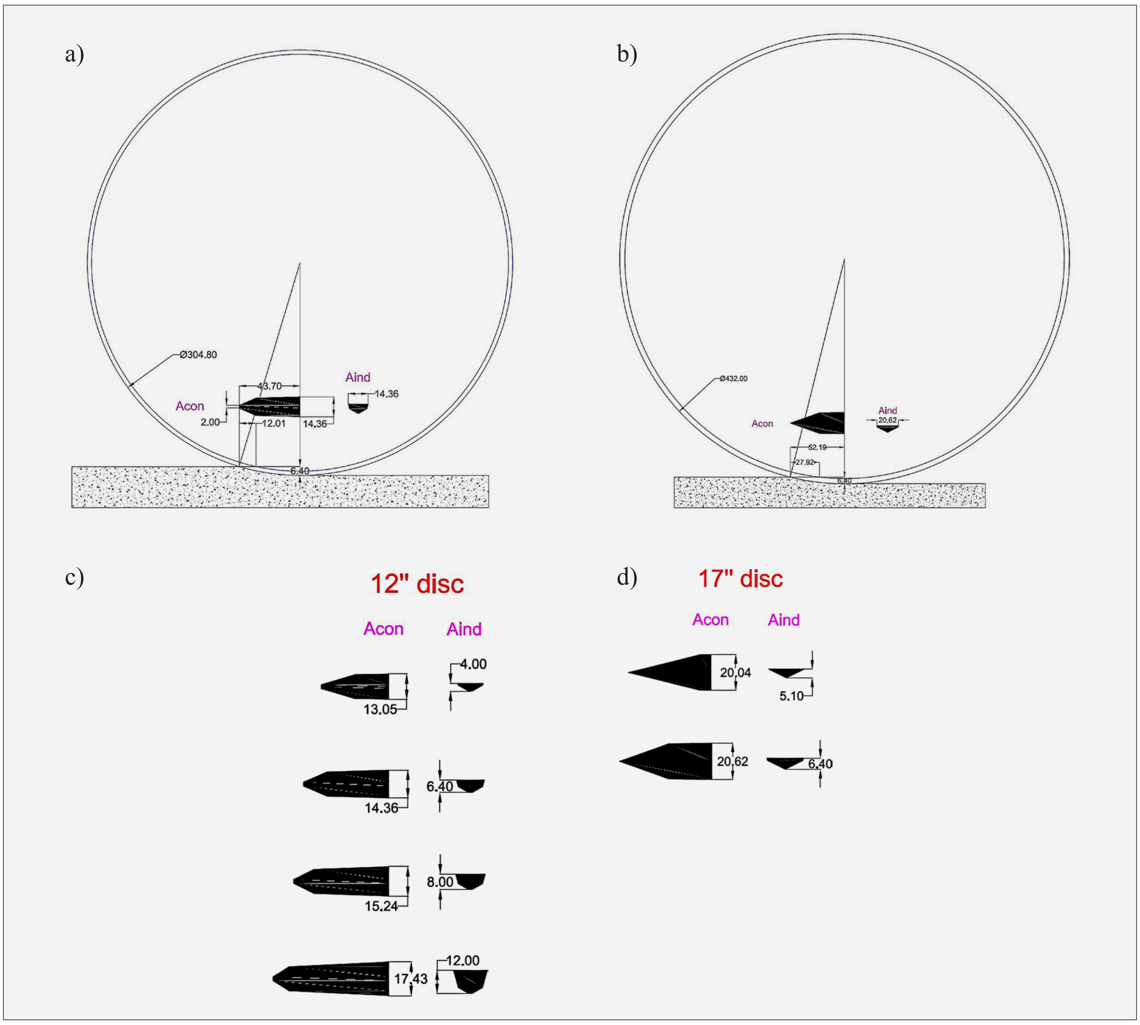

Figure 5: Variation in contact and indentation areas for 12-inch and 17-inch disc cutters at different penetration depths, used to determine cutter–rock interface geometry: (a) example of contact and indentation areas for the 12-inch disc; (b) example of contact and indentation areas for the 17-inch disc; (c) variation of contact and indentation areas for the 12-inch disc; (d) variation of contact and indentation areas for the 17-inch disc

Table 2: Summary of rotary cutting simulation results: input parameters and corresponding normal (Fn), rolling (Fr), and side (Fs) forces, along with calculated contact area (Acon) for each test case

Numerical analysis No.	UCS (MPa)	Cutter diameter (mm)	Spacing (mm)	Penetration (mm)	Radial position (mm)	Fn (kN)	Fr (kN)	Fs (kN)	Acon (mm^2)
1	158	305	25	6.4	1000	106.9	12.3	6.6	513
2	158	305	51	6.4	1000	135.5	14	8	513
3	158	305	76	6.4	1000	154.8	20.9	10.2	513
4	158	305	25	6.4	500	100.6	20.1	10.9	513
5	158	305	51	6.4	500	120.9	22.7	11.6	513
6	158	305	76	6.4	500	128.3	25.3	15.6	513
7	158	305	25	6.4	250	94.9	21.4	14	513
8	158	305	51	6.4	250	110.7	25.2	18.3	513
9	158	305	76	6.4	250	115.1	26.6	21.5	513
10	158	432	25	6.4	1000	143.1	16.1	8.1	772
11	158	432	51	6.4	1000	154.3	18.7	9.6	772
12	158	432	76	6.4	3000	160.9	19.8	1.9	772
13	158	432	25	6.4	500	115.2	17.7	12	772
14	158	432	51	6.4	500	121.6	19.6	14.4	772
15	158	432	76	6.4	500	148.3	25.6	17.5	772
16	158	432	25	6.4	250	105	22.3	19.9	772
17	158	432	51	6.4	250	117.7	25.1	22.3	772
18	158	432	76	6.4	250	136.2	27.3	26.1	772
19	158	432	25	5.1	1000	110	13.6	6.6	532
20	158	432	51	5.1	1000	139.5	15.1	8.3	532
21	158	432	76	5.1	1000	159.4	16.9	9.9	532
22	158	432	25	5.1	500	98	15	11.5	532
23	158	432	51	5.1	500	100.5	16.6	13.1	532
24	158	432	76	5.1	500	118.4	18.3	13.3	532
25	158	432	25	5.1	250	90.7	17.5	17.6	532
26	158	432	51	5.1	250	91.8	20.4	18	532
27	158	432	76	5.1	250	107.3	23.1	23.6	532
28	70	305	25	6.4	1000	47.35	8.9	5.1	513
29	70	305	51	6.4	1000	60.05	11.5	6	513
30	70	305	76	6.4	1000	68.59	13	6.8	513
31	70	305	25	6.4	500	46.2	11.3	7.2	513
32	70	305	51	6.4	500	55	14.8	9.3	513
33	70	305	76	6.4	500	59.7	15.7	10.1	513
34	70	305	25	6.4	250	39.6	15	11	513
35	70	305	51	6.4	250	45.5	16.3	12.4	513
36	70	305	76	6.4	250	49.6	17.5	14.6	513
37	70	432	25	6.4	1000	52.5	10	4.5	772
38	70	432	51	6.4	1000	66.59	11.3	5.6	772
39	70	432	76	6.4	1000	76.06	13.1	7	772
40	70	432	25	6.4	500	50.1	10.8	6.9	772
41	70	432	51	6.4	500	55.9	14.9	9.4	772
42	70	432	76	6.4	500	67.3	18	10.5	772
43	50	305	76	4	1000	42.02	10.9	5.8	347
44	50	305	76	12	1000	59.97	20.6	10	702
45	115	305	76	4	1000	96.64	15.9	8.4	347
46	115	305	76	8	1000	121.1	22.6	11.9	607
47	90	305	25	4	1000	52.8	9.5	4.9	347
48	90	305	51	4	500	61.2	12.7	6.8	347
49	130	305	76	4	250	88.4	19.2	11.5	347
50	130	305	25	8	500	108.6	21.5	13.2	607
51	90	305	76	8	3000	72.5	12	1.1	607
52	130	305	76	8	3000	95.8	15.5	1.5	607
53	90	432	25	4	1000	68.4	11.2	6	328
54	90	432	51	4	500	77.9	14.6	8.1	328
55	130	432	76	4	250	110.2	20.8	12.9	328
56	130	432	25	5.1	500	120.7	18.2	11.4	532
57	90	432	76	5.1	3000	98.6	13.5	1.2	532
58	130	432	76	5.1	3000	125.4	17	1.6	532

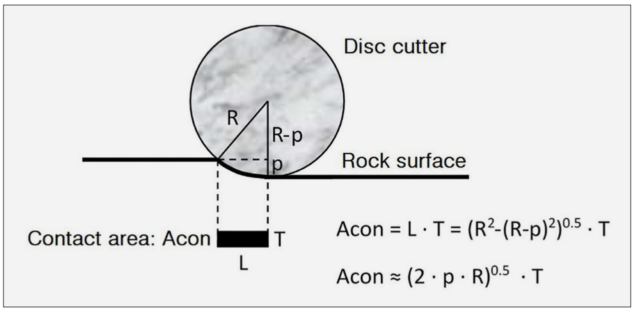

Figure 6: Simplified geometric method for estimating disc–rock contact area (A_{con}), based on cutter tip width, radius, and penetration depth

tation profiles in AutoCAD, accounting for penetration depth and disc diameter. The variation in contact and indentation areas for both 17-inch and 12-inch discs under different penetration scenarios is shown in **Figure 5**.

The outcomes of 58 rotary cutting simulations are summarised in **Table 2**. Each entry reports the input parameters and resulting force components, together with the computed contact area. The results reveal consistent trends: greater UCS and larger contact areas generally lead to increased cutting forces. Conversely, forces tend to decrease as the cutter's radial position increases, owing to reduced curvature-induced resistance.

A simplified geometric approach for estimating the contact area, as expressed in **Equation 1**, is presented in **Figure 6**.

$$A_{con} = T \cdot L = T \cdot (2 \cdot R \cdot p)^{0.5} \qquad (1)$$

Where:

A_{con} – disc contact area (mm²),
T – cutter tip width (mm),
L – horizontal contact area length (mm),
R – cutter radius (mm),
p – cutter penetration (mm).

This formulation provides a practical tool for estimating contact area in future parametric studies.

3.2. Simple regression analysis

To explore the influence of individual parameters on disc cutter forces, a series of simple regression analysis were performed. These analyses focused on identifying direct relationships between input variables – such as rock compressive strength, cutter spacing, radial position, and contact area – and the resulting force components: normal (Fn), rolling (Fr), and side (Fs).

The results indicate a strong positive correlation between UCS and normal force, consistent across both 12-inch and 17-inch disc configurations, as shown in **Figure 7**. The coefficient of determination (R^2) was greater than 0.70, confirming the predictive strength of this relationship. This trend aligns with findings from previous cutting studies (**Snowdon et al., 1982; Jeong et al., 2023**).

Cutter spacing also showed a direct influence on all three force components. As spacing increased, the magnitude of Fn, Fr, and Fs rose accordingly. This pattern was observed for both disc sizes and across different rock strengths, as shown in **Figures 8** through **13**.

The effect of radial installation position on normal force was more complex. Initially, Fn increased with radial distance, peaking around 1000 mm, before declining beyond that point. This behaviour is attributed to the curvature of the cutting path – greater curvature near the centre enhances rolling and side forces, thereby reducing the normal force required for rock breakage, as shown in **Figure 14**.

Contact area (A_{con}) exhibited a modest correlation with normal force, as shown in **Figure 15**. While larger contact areas generally led to higher Fn values, the relationship was weaker than that observed for UCS. No significant correlation was found between Acon and the rolling or side forces.

In summary, UCS emerged as the most influential factor in predicting cutter forces, followed by spacing and contact area. Radial position introduced nonlinear effects due to geometric curvature, underscoring the need for multi-variable modelling in rotary cutting simulations.

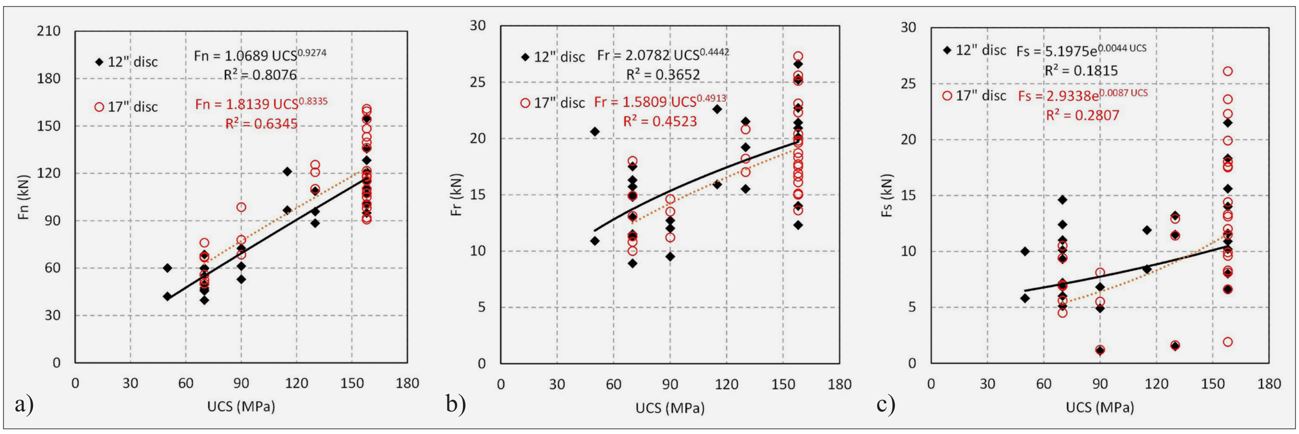

Figure 7: Influence of UCS on disc cutter forces – (a) normal force (Fn), (b) rolling force (Fr), and (c) side force (Fs) – for both 12-inch and 17-inch discs, showing a strong positive correlation

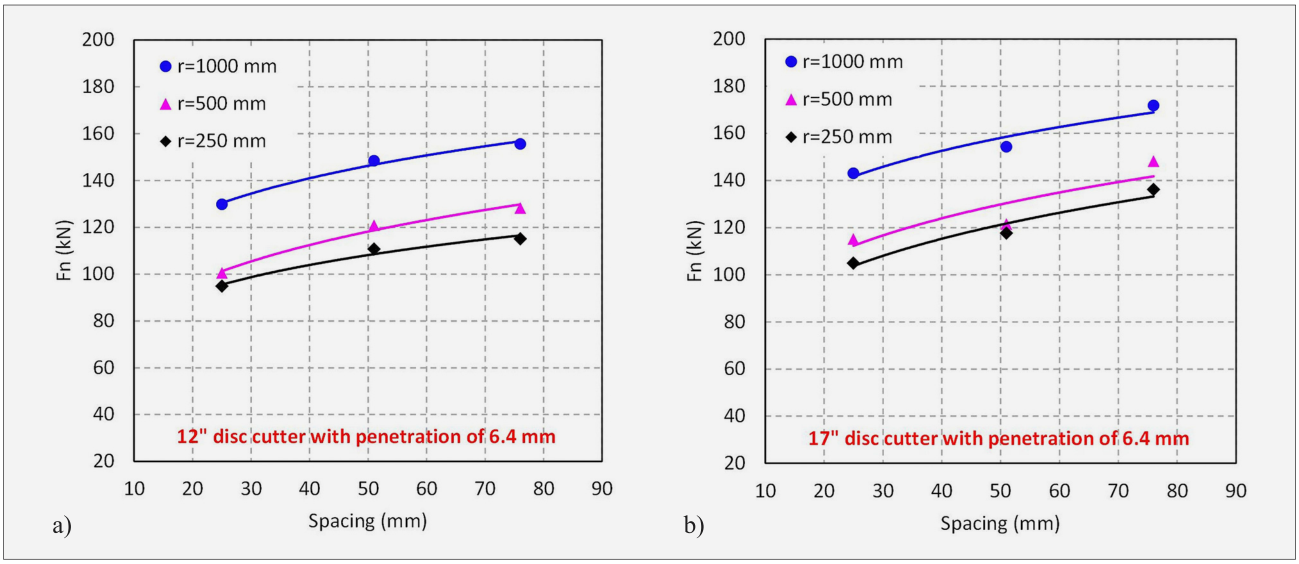

Figure 8: Variation in normal force with cutter spacing and radial position for simulations conducted on rock with a UCS of 158 MPa using (a) 12-inch and (b) 17-inch disc cutters.

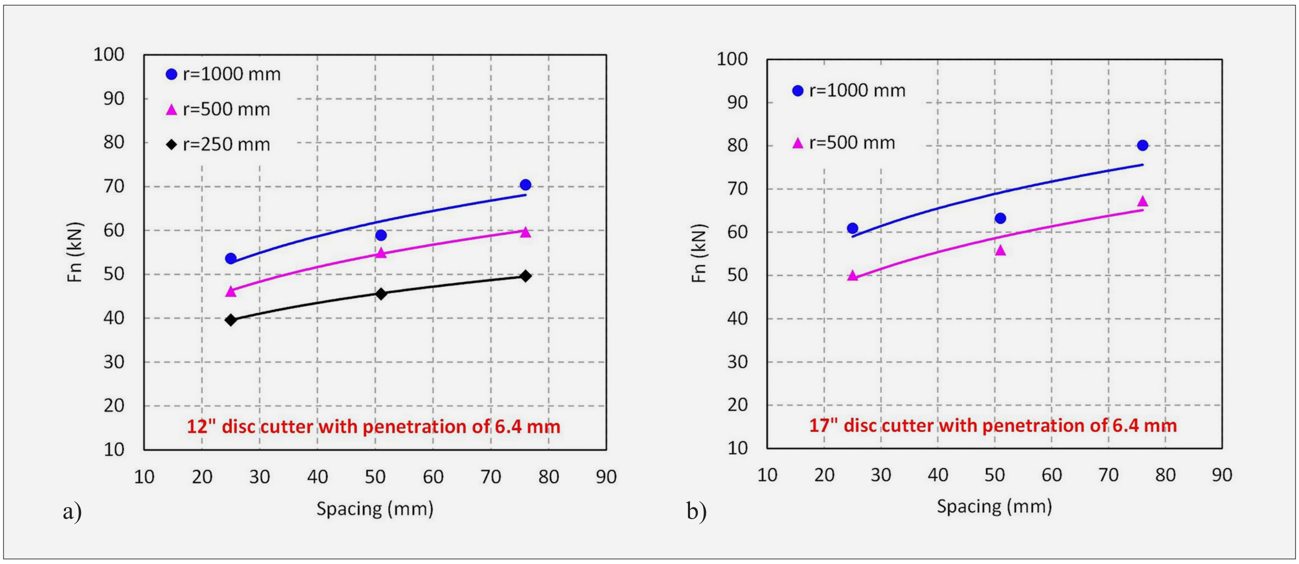

Figure 9: Relationship between cutter spacing, radial position, and normal force for simulations conducted on rock with a UCS of 70 MPa using (a) 12-inch and (b) 17-inch disc cutters.

3.3. Multiple regression analysis

To establish predictive relationships for disc cutter forces under rotary cutting conditions, multiple regression analysis was performed using the dataset generated from 58 validated LS-DYNA simulations. These simulations encompassed a wide range of input parameters, including UCS, cutter–rock contact area (A_{con}), and radial installation position (R), each of which had demonstrated statistical relevance in the preceding single-variable analyses. The objective was to formulate empirical equations for estimating the three primary force components – normal force (Fn), rolling force (Fr), and side force (Fs) – based on these influential variables. This approach enables a more comprehensive understanding of how geological and geometric factors interact to affect cutter performance in rotary TBM operations.

To strengthen the statistical robustness of the regression models and to meet the assumption of normally distributed residuals, a natural logarithmic transformation was applied to all variables prior to analysis. Linear regression was then performed on the log-transformed data. Although the statistical fitting procedure itself is linear in the transformed space, the back-transformed equations are non-linear in their original form. This approach stabilizes variance, improves the normality of residuals, and linearizes multiplicative relationships during estimation, while ultimately yielding non-linear predictive equations that better capture the complex interactions between geological and mechanical parame-

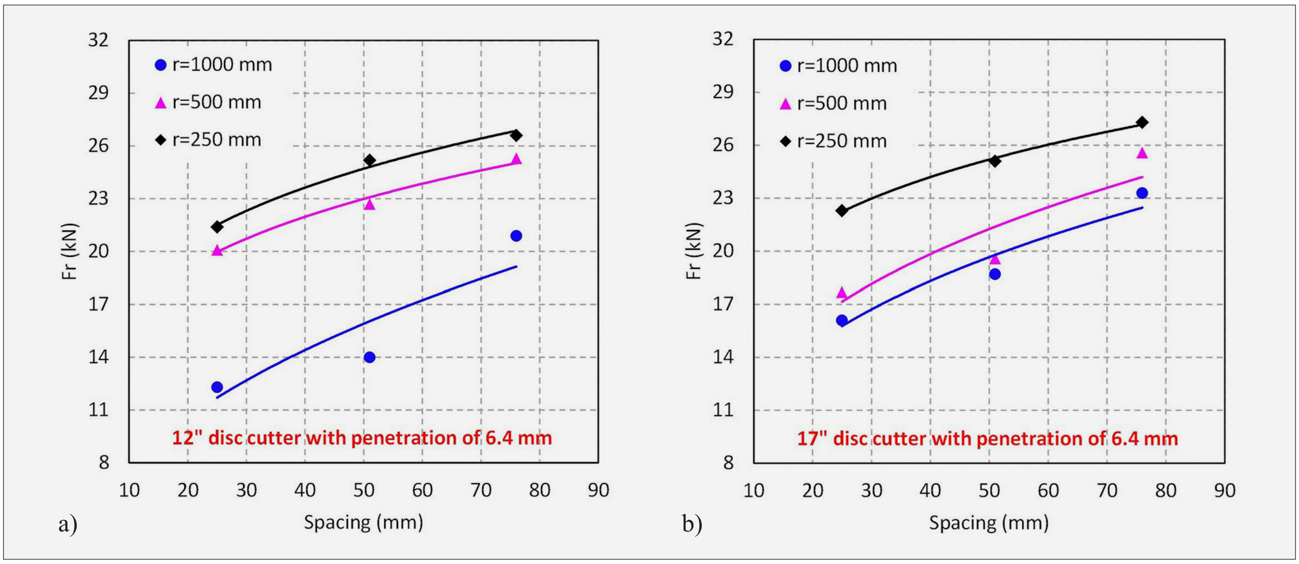

Figure 10: Rolling force trends as a function of cutter spacing and radial position for rock with 158 MPa compressive strength using (a) 12-inch and (b) 17-inch disc cutters

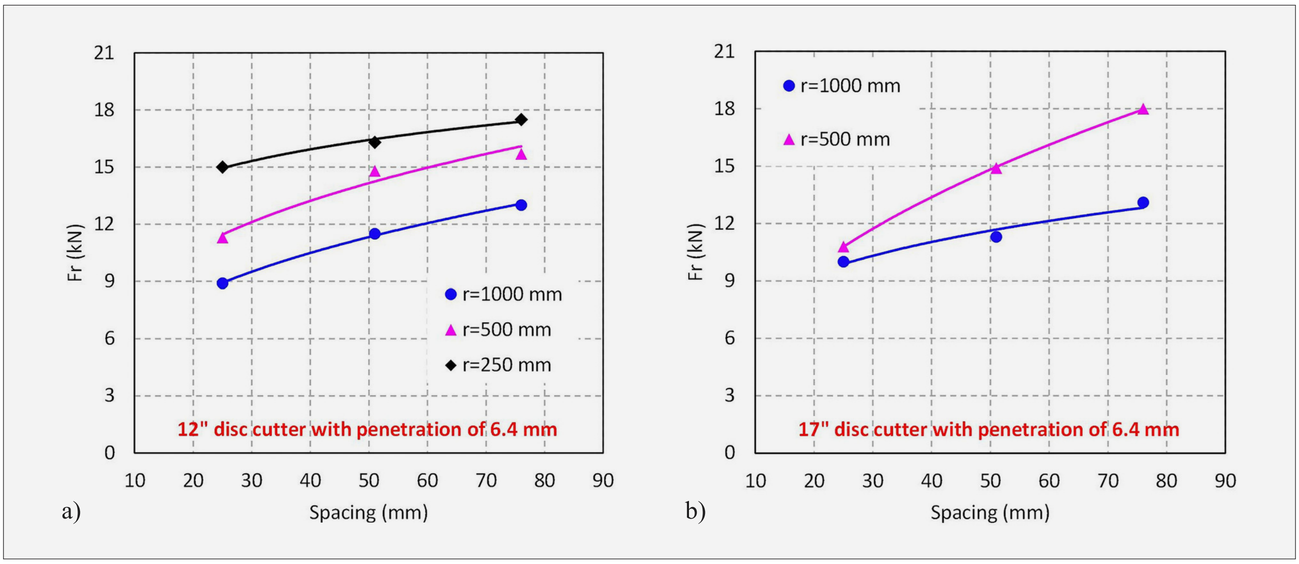

Figure 11: Rolling force variation with spacing and radial location for rock with 70 MPa compressive strength using (a) 12-inch and (b) 17-inch disc cutters

ters. The use of logarithmic transformation followed by linear regression is consistent with established practice in TBM performance modelling, including the development of the Colorado School of Mines (CSM) model (**Rostami, 1997**).

During the multiple regression process, each input variable was assessed for inclusion based on two statistical thresholds. First, a p-value less than 0.05 was required to confirm a meaningful relationship between the predictor and the corresponding force component, ensuring that the variable contributed significantly to the model. Second, the variance inflation factor (VIF) for each parameter had to remain below 10, which indicates low multicollinearity and confirms that the predictors are not excessively correlated with one another. These criteria ensured that the final equations were both statistically valid and structurally stable, minimizing distortion from redundant or non-informative variables.

The optimised regression formulas for three key outputs – cutter normal force (F_n), rolling force coefficient (k_r), and side force coefficient (k_s) – are presented in **Table 3**. These models were developed using the natural logarithms of the target variables – $Ln(F_n)$, $Ln(k_r)$, and $Ln(k_s)$ – to enhance linearity and normalize error distributions. Predictor variables were also log-transformed to maintain consistency and improve model fit. The regression procedure employed both step-forward selection and best-subset evaluation to identify the most statistically robust combinations of predictors for each force component. All coefficients are reported as esti-

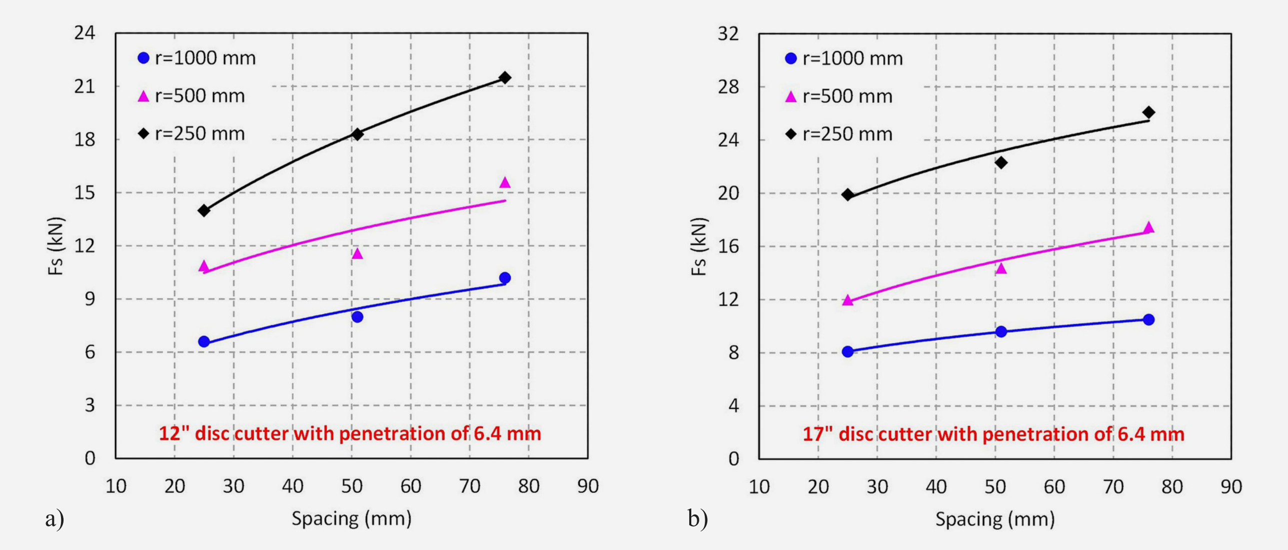

Figure 12: Side force behaviour across different cutter spacings and radial positions for rock with 158 MPa compressive strength using (a) 12-inch and (b) 17-inch disc cutters

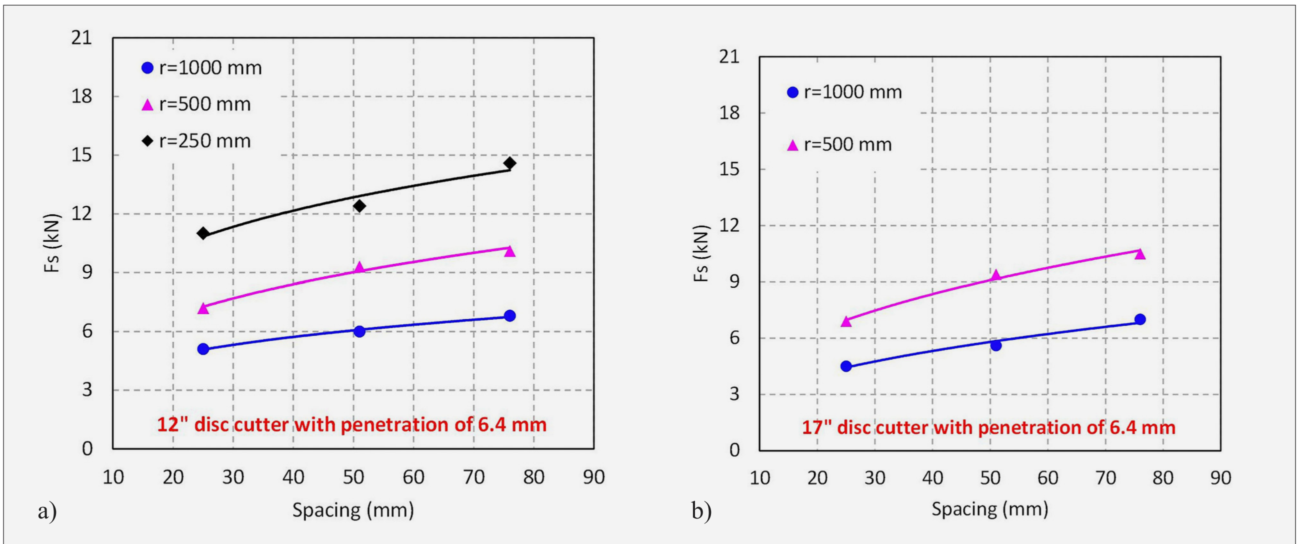

Figure 13: Side force response to spacing and radial placement for rock with 70 MPa compressive strength using (a) 12-inch and (b) 17-inch disc cutters

mates with their standard errors and 95% confidence intervals.

The coefficient of determination (R^2) is calculated by the software using the formula of R^2 = (TSS-RSS)/TSS, where TSS denotes the total sum of squares, representing the cumulative squared deviation of observed values from their mean, and RSS is the residual sum of squares, quantifying the squared differences between observed and predicted values. This metric reflects the proportion of variance in the dependent variable explained by the model.

Additionally, the term $(1 - \exp(-0.00872\, r))$, which appears in the final Fn formula, was extracted from the simple regression analysis of radial position effects, as illustrated in **Figure 14**. This exponential term captures the nonlinear influence of cutter radius on normal force, particularly in the outer zones of the cutterhead.

A direct comparison between the predicted cutting forces – calculated using the regression formulas in **Table 3** – and the actual values obtained from the LS-DYNA simulations is shown in **Figure 16**. The data points align closely with the 1:1 reference line, indicating strong agreement between modeled and observed results. To quantify this agreement, model accuracy was assessed using root mean square error (RMSE), mean absolute error (MAE), and mean absolute percentage error (MAPE). For normal force (Fn), the regression model achieved RMSE = 17.70 kN, MAE = 13.56 kN, and MAPE = 12.16%; for rolling force (Fr), RMSE = 2.39 kN, MAE = 1.82 kN, and MAPE = 10.73%; and for side force (Fs), RMSE = 1.68 kN, MAE = 1.15 kN, and MAPE = 18.34%. These quantitative results, together with the visual validation in **Figure 16**, confirm the reli-

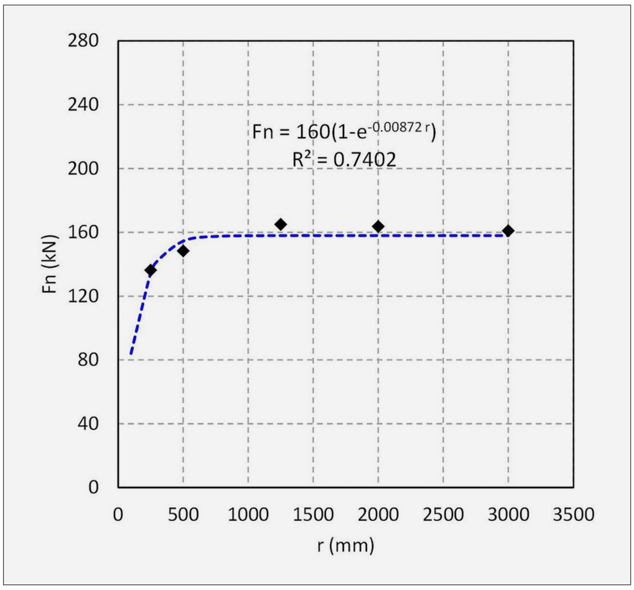

Figure 14: Nonlinear relationship between cutter installation radius and normal force for a 17-inch disc operating in rock with 158 MPa compressive strength

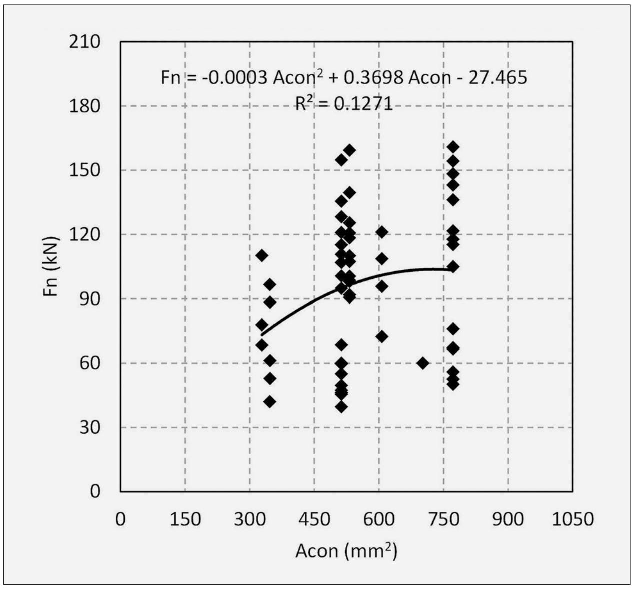

Figure 15: Correlation between disc–rock contact area and normal force, indicating a weaker but positive trend compared to other parameters

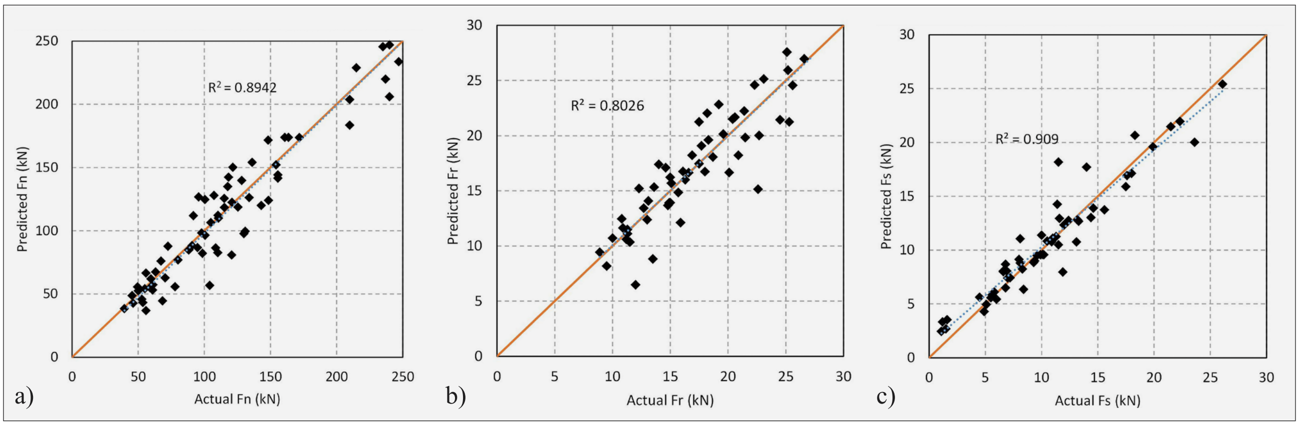

Figure 16: Comparison between predicted cutter forcesversus calculated ones using regression formulas – and actual values from LS-DYNA simulations for (a) Fn, (b) Fr, and (c) Fs, showing strong alignment along the 1:1 reference lines.

Table 3: Final regression equations for estimating cutter normal force (F_n), rolling force coefficient (k_r), and side force coefficient (k_s), derived using natural log-transformed variables and stepwise selection methods

No.	Regression formula*	R²	Parameter Estimates (with SE and 95% CI)
1	$Ln(F_n) = b_0 + b_1\ \mathrm{Ln}(UCS)$ $+b_2\ Ln(A_{con}) + b_3\ \mathrm{Ln}(\mathrm{S})$ $+b_4\ \mathrm{Ln}\ (1 - \exp(-0.00872\ r))$	0.8942	b_0 : -4.6725 (SE = 0.0119, 95% CI [-4.697, -4.649]) b_1 : 0.9997 (SE = 0.0038, 95% CI [0.992, 1.007]) b_2 : 0.4996 (SE = 0.0030, 95% CI [0.494, 0.506]) b_3 : 0.3316 (SE = 0.0048, 95% CI [0.322, 0.341]) b_4 : 1.0082 (SE = 0.0674, 95% CI [0.892, 1.162])
2	$Ln(k_r) = b_0 + b_1\ \mathrm{Ln}(UCS) + b_2\ Ln(r))$	0.8026	b_0: 3.8410 (SE = 0.0248, 95% CI [3.791, 3.890]) b_1 : -0.5008 (SE = 0.0072, 95% CI [-0.515, -0.486]) b_2 : -0.4994 (SE = 0.0088, 95% CI [-0.517, -0.482])
3	$Ln(k_s) = b_0 + b_1\ \mathrm{Ln}(UCS) + b_2\ Ln(r))$	0.9090	b_0: 5.2701 (SE = 0.0365, 95% CI [5.196, 5.342]) b_1 : -0.5002 (SE = 0.0077, 95% CI [-0.516, -0.485]) b_2 : -0.8004 (SE = 0.0054, 95% CI [-0.811, -0.789])

* In these formulas, F_n is cutter normal force in kN, F_r is cutter rolling force in kN, UCS is uniaxial compressive strength of the rock in MPa, Acon is the contact area of the disc with the rock in mm2, S is cutter spacing in mm, r is the radial position of the cutter in mm, k_r is the cutter coefficient for the rolling force, and k_s is the cutter coefficient for the side force.

Table 4: Measured cutter forces from RCM tests on Korean granite (**Shin et al., 2024**) and predicted values from regression equations developed in this study.

Penetration (mm)	Radial position (mm)	Fn (RCM) (kN)	Fn predicted (kN)	Fr (RCM) (kN)	Fr predicted (kN)	Fs (RCM) (kN)	Fs predicted (kN)
4	200	235.0	224.90	66	70.35	63.0	59.92
5	200	241.0	239.94	69	72.15	66.0	61.45
4	300	243.0	246.72	67	59.40	43.0	44.80
5	300	248.0	262.20	55	60.62	48.0	45.72
4	600	255.0	256.90	50	44.08	24.3	27.00
5	600	273.4	271.64	45	47.26	22.0	28.95

Table 5: Aggregate error metrics for comparison of predicted and measured forces in RCM tests on Korean granite

Force component	RMSE (kN)	MAE (kN)	MAPE (%)
Fn	6.24	5.33	2.17
Fr	7.84	6.56	10.79
Fs	3.00	2.57	7.03

ability of the regression equations and their applicability for estimating cutter forces under varying geological and geometric conditions.

The formulas presented in **Table 3** are in natural logarithmic format. The power format of these formulas are presented in **Equations 2** to **4**.

$$F_n = 0.009349\ UCS\ A_{con}^{\frac{1}{2}}\ S^{\frac{1}{3}}\ (1 - \exp(-0.00872\ r)) \quad (2)$$

$$k_r = \frac{F_r}{F_n} = \frac{46.6}{UCS^{\frac{1}{2}}\ r^{\frac{1}{2}}} \quad (3)$$

$$k_s = \frac{F_s}{F_n} = \frac{194.4}{UCS^{\frac{1}{2}}\ r^{\frac{4}{5}}} \quad (4)$$

3.4. Validation against RCM tests on Korean granite

To further assess the generality and predictive capability of the proposed regression equations, an additional validation was performed using the full-scale rotary cutting machine (RCM) tests reported by **Shin et al. (2024)**. These experiments were conducted on Hwandeung granite with a uniaxial compressive strength of 205 MPa using a 17-inch disc cutter with a 21 mm tip width, a cutter spacing of 100 mm, and penetration depths of 4 mm and 5 mm. The RCM platform recorded the triaxial cutter forces during rotary cutting at radial positions of 200, 300, and 600 mm, providing an independent dataset for evaluating the performance of the developed force-prediction equations.

The measured normal, rolling, and side forces from the RCM tests together with the corresponding predicted values obtained from **Equations 2** to **4** are reported in **Table 4**. As shown in **Table 4**, the predicted normal forces closely match the experimental values across all radii and penetration depths, with deviations typically below 3%. The rolling force predictions also follow the experimental trend, although slightly higher deviations are observed at larger radii, which is consistent with the higher variability of Fr reported in rotary cutting studies. The predicted side forces reproduce both the magnitude and the decreasing trend with increasing radius, demonstrating that the model captures the radial dependence of lateral loading.

To quantify predictive accuracy, the root mean square error (RMSE), mean absolute error (MAE), and mean absolute percentage error (MAPE) were computed for each force component using the paired experimental and predicted values reported in **Table 4**. The values presented in **Table 5** represent aggregate statistics calculated across all penetration depths (4 and 5 mm) and radial positions (200, 300, and 600 mm), thereby providing an overall measure of model performance rather than case-by-case results. For the normal force, the RMSE and MAE were 6.24 kN and 5.33 kN, respectively, with a MAPE of only 2.17%, confirming the high reliability of the proposed formulation for Fn. The rolling force yielded RMSE and MAE values of 7.84 kN and 6.56 kN, with a MAPE of 10.79%, which is acceptable given the inherent variability of Fr observed in rotary cutting tests. The side force showed similarly strong agreement, with RMSE and MAE values of 3.00 kN and 2.57 kN and a MAPE of 7.03%, demonstrating that the model reproduces both the magnitude and radial trend of Fs with satisfactory accuracy.

The close agreement between the measured and predicted forces, combined with the consistently low error metrics, confirms that the proposed regression equations are capable of reproducing both the magnitudes and the radial trends of cutter forces observed in full-scale rotary cutting tests. This validation provides strong evidence that the equations can be reliably applied in practice for cutterhead layout optimization, accurate force estimation, and performance prediction in hard-rock TBM tunnelling.

4. Discussion

The results of the rotary cutting simulations and regression analyses provide valuable insight into the mechanical behaviour of disc cutters under varying geological and geometric conditions. By adopting an ln-linear regression framework, the present study ensures that the power-law relationships of influential parameters and cutter forces are captured transparently. The narrow confidence intervals observed for most coefficients confirm the stability of the ln-linear models, while wider intervals for radial effects highlight areas requiring further data expansion. The empirical models demonstrate that UCS is the most influential parameter across all force components, particularly for normal force (Fn), where its contribution is both statistically and physically dominant. This finding is consistent with established cutting theories and prior experimental studies (**Snowdon et al., 1982; Rostami, 1997; Jeong et al., 2023**). In the dataset, Fn values increased from 42 kN at UCS = 50 MPa to over 160 kN at UCS = 158 MPa, confirming the strong positive correlation observed in **Figure 7**.

The inclusion of contact area (A_{con}) and radial installation position (r) in the regression models enhances predictive capability. While A_{con} contributes positively to all force components, its effect is secondary compared to UCS. For example, increasing penetration from 4 mm to 12 mm expanded A_{con} from 347 mm² to 702 mm², raising Fn from 42 kN to nearly 60 kN (**Table 2**, analyses 43–44). The influence of radial position is more nuanced: Fn decreases as the cutter's installation radius decreases, whereas Fr and Fs increase owing to the reduced radius of curvature. This behaviour is captured effectively by the exponential term (1 – exp(–0.00872R)), which reflects the nonlinear relationship between cutter radius and normal force (see **Figure 14**). The use of logarithmic transformation in the regression process further stabilised variance and improved model fit, producing equations that offer practical tools for estimating cutter forces in rotary TBM operations. Their accuracy was validated through comparison with simulation outputs, as shown in **Figure 16**, where predicted values closely matched actual results.

The regression-based force prediction formulas demonstrate strong agreement with recent full-scale rotary cutting tests. **Huang et al. (2024) and Deng et al. (2024)** reported that normal forces increase with cutting radius in granite, while side forces exhibit more complex behaviour. The simulations presented here captured the transition of side forces from higher values near the centre to reduced magnitudes at larger radii, consistent with those observations. The incorporation of radial position as a primary variable distinguishes this work from previous CSM-based models. **Zhang et al. (2024)** proposed modifications to the CSM model incorporating installation radius and synergistic effect factors using MatDEM simulations, but their calibration relied primarily on linear cutting data. In contrast, the SPG-based rotary cutting simulations presented here provide a direct representation of the circular trajectories experienced by disc cutters during TBM operation, producing validated regression formulas across 58 scenarios.

This study also advances numerical modelling approaches by applying the SPG mesh-free method to large-radius rotary cutting. Previous FEM-SPH studies (**Geng et al., 2022; Xiao et al., 2017**) primarily focused on dual-cutter interaction or small-radius rotary cutting. The validated SPG framework successfully simulated single-cutter rotary cutting at radii up to 3000 mm, bridging the gap between laboratory linear cutting tests and full-scale TBM cutterhead operation. Unlike previous models that primarily emphasize normal and rolling forces, the regression equations developed in this study predict all three force components – normal, rolling, and side – individually for both the center and face zones. This comprehensive formulation provides the complete force state required for cutterhead structural analysis and cutter bearing selection. The force components associated with the gauge area are inherently more complex and have been addressed in detail by **Farrokh et al. (2024a)**.

The importance of proper material model calibration is well documented in rock mechanics. **Hajibagherpour et al. (2020)** demonstrated that discontinuities significantly affect fracture patterns around blastholes, while **Aftabi and Ahangari (2023)** showed that microparameters in particle flow code models critically influence predicted strength properties. The use of the RHT material model with parameters validated against Colorado red granite cutting tests (**Xie et al., 2017; Farrokh et al., 2024b**) ensured that the material response – including tensile cracking, compressive crushing, and strain-rate effects – was accurately represented in the rotary cutting simulations.

Several recent studies have addressed disc cutter wear prediction, highlighting that wear increases contact area and alters force distribution (**Sabri & Goshtasbi, 2024; Wang et al., 2024**). The force prediction formulas developed in this study were derived for sharp (unworn) cutters operating in intact rock, thereby establishing a baseline against which force variations induced by cutter wear can be quantitatively assessed. Future extensions could incorporate contact area growth due to wear, building upon the fundamental relationships established in this study. These findings have direct implications for cutterhead design and performance forecasting. By quantifying the influence of UCS, contact geometry, and cutter placement, cutter layout can be optimised to balance force distribution, reduce wear, and improve excavation efficiency. Moreover, the regression models can serve as input for higher-level TBM performance simulations, integrating geological variability with mechanical response.

It is important to recognize that field TBM cutting occurs under in-situ stress conditions that influence rock fracture behavior. **Moomivand et al. (2022)** demonstrated that the prevailing stress state has a significant impact on excavation stability. The present focus on intact rock under unconfined conditions establishes fundamental force relationships that serve as a baseline for future investigations incorporating confining stress effects. The modular structure of the regression formulas further facilitates extensions to include in-situ stress as an additional variable. Beyond stress considerations, subsequent research may also address cutter tip geometry, rock anisotropy, and dynamic loading conditions. Machine learning approaches could be explored to capture nonlinear interactions that extend beyond the capabilities of traditional regression.

Overall, this study introduces the first regression-based force prediction formulas that explicitly integrate radial position, contact area, and rock strength across center and face cutterhead zones. The application of the SPG mesh-free method to large-radius rotary cutting enables accurate simulation of single-cutter trajectories up to 3000 mm, thereby bridging the gap between laboratory-scale linear cutting tests and full-scale TBM operation. The comprehensive prediction of normal, rolling, and side forces provides the complete force state required for cutterhead structural analysis and bearing design. These contributions extend beyond the limitations of linear cutting test data, directly supporting engineering tasks such as cutter layout optimization, torque and thrust estimation, and bearing capacity verification. The study thus establishes a robust foundation for data-driven cutter force estimation and cutterhead design in hard rock tunnelling.

5. Conclusions

This study has presented a systematic numerical investigation into the rotary cutting behaviour of disc cutters, combining LS-DYNA simulations with regression-based modelling. A total of 58 simulation cases were examined, encompassing variations in rock strength, cutter geometry, penetration depth, spacing, and radial installation position. The RHT constitutive model was employed to represent the mechanical response of Colorado red granite under dynamic loading, enabling a realistic depiction of rock fragmentation and force generation.

The findings confirm that UCS is the dominant factor influencing cutter forces, particularly the normal force (Fn). Contact area and radial installation position also exert significant effects, with radial variation introducing nonlinear behaviour attributable to changes in curvature and velocity gradients across the cutterhead. Multiple regression analyses produced predictive equations for Fn, Fr, and Fs, with coefficients of determination (R^2) exceeding 0.80, thereby demonstrating strong statistical reliability.

The final regression formulas, derived through natural logarithmic transformations and validated against simulation data. These models support cutterhead layout optimisation, performance forecasting, and parametric sensitivity studies in hard-rock tunnelling. Notably, the exponential term introduced for radial influence improves the accuracy of Fn prediction by capturing geometric effects that are not addressed in conventional linear cutting models.

Future research should extend this framework by incorporating additional variables such as cutter tip shape, rock anisotropy, and dynamic tool–rock interactions. Integration with machine-learning techniques may further enhance predictive accuracy and adaptability across diverse geological conditions. Overall, the methodology and results contribute to advancing reproducible, data-driven approaches for cutterhead design and performance modelling in mechanised tunnelling.

Acknowledgements

This research was financially supported by Tunnel Saz Machine Company under Project No. 100404519. The authors extend their sincere appreciation to Mr. Saheb, CEO of the company, for his generous backing throughout the study. Gratitude is also expressed to the entire Tunnel Saz Machine team for their valuable assistance in data preparation, technical coordination, and information gathering during the course of this work.

Funding

This research was supported by the Tunnel Saz Machine Company (Project number: 100404519).

Data Availability

No data has been used or produced during the preparation of this manuscript.

Competing interests

The contact author has declared that none of the authors have any competing interests.

6. References

Arbabsiar, M. H., Ebrahimi Farsangi, M. A., & Mansouri, H. (2020). A new model for predicting the advance rate of a Tunnel Boring Machine (TBM) in hard rock conditions. *Rudarsko-geološko-naftni zbornik*, 35 (2), 57-74. https://doi.org/10.17794/rgn.2020.2.6

Armaghani, D. J., Yagiz, S., Mohamad, E. T., & Zhou, J. (2021). Prediction of TBM performance in fresh through weathered granite using empirical and statistical approaches. *Tunnelling and Underground Space Technology*, 118, 104183. https://doi.org/10.1016/j.tust.2021.104183

Chen, W. F. (2007). Plasticity in Reinforced Concrete. J. Ross Publishing. ISBN 1932159774.

Deng, L.-C., Li, X.-Z., Xu, W., Zhang, C., Zhuang, Q.-W., Li, F.-Q., & Zhou, Q. (2024). Full-scale test of disc cutter rotary cutting in TBM tunnelling: A case study of Mawan granite in Shenzhen, China. *Geomechanics and Geophysics for Geo-Energy and Geo-Resources*, 10, Article 167. https://doi.org/10.1007/s40948-024-00886-3

Entacher, M., & Lassnig, K. (2012). Findings from disc cutting tests on alpine lithologies / Erkenntnisse aus Diskenschneidversuchen an alpinen Lithologien. *Geomechanics and Tunnelling*, 5(5), 547–556. https://doi.org/10.1002/geot.201200041

Farrokh, E. (2022). Using field data and operational constraints to maximize hard rock TBM penetration and advance rates. *Tunnelling and Underground Space Technology*, 125, 104506. https://doi.org/10.1016/j.tust.2022.104506

Farrokh, E., Rokhy, H. & Lotfi, D. (2024a) Evaluation of side forces for gauge cutters through LS-DYNA 3D numerical simulations. *Arabian Journal of Geosciences* 17, 211. https://doi.org/10.1007/s12517-024-12019-x

Farrokh, E., Rokhy, H., & Lotfi, D. (2024b). On the application of RHT model and SPG algorithm for the analysis of rock cutting process. *Simulation Modelling Practice and Theory*, 136(3), 103012. https://doi.org/10.1016/j.simpat.2024.103012

Farrokh, E., Kim, D. Y., & Kyung, S. B. (2015). Rotary cutting test for hard rock TBM performance evaluation. *World Tunneling Conference*, Dubrovnik, Croatia.

Geng, Q., Wei, Z. Y., & Ren, J. H. (2017). New rock material definition strategy for FEM numerical analysis of the rock cutting process by TBM disc cutters. *Tunneling and Underground Space Technology*, 65, 179–186. https://doi.org/10.1016/j.tust.2017.03.001

Geng, Q., Shi, M., Liu, X., Wei, Z., & Chen, R. (2022). Tunnel boring machine (TBM) cutter spacing design based on simulations of rock breaking process using a FEM-SPH coupling method. In J. Tan (Ed.), Advances in Mechanical Design (pp. 2175-2194). Springer. https://doi.org/10.1007/978-981-16-7381-8_136

Huang, X., Tang, M., Wang, S., Zhai, Y., Zhuang, Q., Zhang, C., & Lei, Q. (2024). Assessing cutter-rock interaction during TBM tunnelling in granite: Large-scale standing rotary cutting tests and 3D DEM simulations. *Journal of Rock Mechanics and Geotechnical Engineering*, 16(10), 3595–3615. https://doi.org/10.1016/j.jrmge.2024.01.016

Jaime, M. (2011). Numerical modelling of rock cutting for mechanical excavation in hard rock conditions (Doctoral dissertation, University of Pittsburgh).

Jeong, H., Cho, J.-W., Tumac, D., & Jeon, S. (2020). Rock cutting numerical analysis of point attack picks using the smooth particle hydrodynamics (SPH) technique. *Applied Sciences*, 10(15), 5314. https://doi.org/10.3390/app10155314

Jeong, H., Choi, S., & Lee, Y. K. (2023). Evaluation of cutting performance of a TBM disc cutter and Cerchar abrasivity index based on the brittleness and properties of rock. *Applied Sciences*, 13(4), 2612. https://doi.org/10.3390/app13042612

Jeong, Ho-Young, Jeon, Seokwon, & Cho, Jung Woo. (2013). A numerical study on rock cutting by a TBM disc cutter using SPH code. Journal of Korean *Tunnelling and Underground Space Association*, 15(3), 345–356. https://doi.org/10.9711/KTAJ.2013.15.3.345

Khosravi, M., Ramezanzadeh, A., & Zare, S. (2021). Evaluation of disc cutter performance in rock cutting process using 3D finite element method. *Numerical Methods in Civil Engineering*, 5(3), 1–12. https://doi.org/10.52547/NMCE.5.3.1

Ko, T. Y., Yoon, H. J., & Son, Y. J. (2014). A comparative study on the TBM disc cutter wear prediction model. *Journal of Korean Tunnelling and Underground Space Association*, 16(6), 533–542. https://doi.org/10.9711/KTAJ.2014.16.6.533

Palassi, M., Koohmishi, M., & Jangi, M. (2025). Effect of geometrical characteristics of TBM disc cutter on rock excavation: A focus on cutter diameter and cutter tip profile. *Geotechnique Letters*, 15(2), 136–142. https://doi.org/10.1680/jgele.24.00102

Pan, Y., Liu, Q., Liu, J., Kong, X., Peng, X., & Liu, Q. (2021). Investigation on disc cutter behaviours in cutting rocks of different strengths and reverse estimation of rock strengths from experimental cutting forces. *European Journal of Environmental and Civil Engineering*, 25(1), 1–27. https://doi.org/10.1080/19648189.2018.1512904

Riedel, W., Kawai, N., & Kondo, K. I. (2009). Numerical assessment for impact strength measurements in concrete materials. *International Journal of Impact Engineering*, 36(2), 283–293. https://doi.org/10.1016/j.ijimpeng.2007.12.012

Rostami, J. (1997). Development of a force estimation model for rock fragmentation with disc cutters through theoretical modelling and physical measurement of crushed zone pressure (Doctoral dissertation, Colorado School of Mines). Colorado School of Mines, Golden, CO, USA, p. 249.

Sabri, M., & Goshtasbi, K. (2024). Evaluation of the effect of TBM disc cutter wear on rock cutting efficiency. *Geomechanics and Tunnelling*, 17(2), 252-262. https://doi.org/10.1002/geot.202300015

Salimi, A., Rostami, J., Moormann, C., & Hassanpour, J. (2022). Introducing tree-based regression models for prediction of hard rock TBM performance with consideration of rock type. *Rock Mechanics and Rock Engineering*, 55(11), 4869–4891. https://doi.org/10.1007/s00603-022-02868-x

Schlicke, M., Nübel, K., Wannenmacher, H., Amann, F., & Marcher, T. (2024). The thrust-penetration gradient: Decoding geomechanical dynamics and TBM response (Paper No. ARMA-2024-0423). Presented at the 58th U.S. Rock Mechanics/Geomechanics Symposium, Golden, Colorado, USA.

Shin, Y. J., Farrokh, E., Jung, J., Lee, J., & Kang, H. (2024). A study of rotary cutting machine (RCM) performance on Korean granite. *Engineering Computations*, 41(1), 155–182. Emerald Publishing Limited. https://doi.org/10.1108/EC-08-2023-0462

Snowdon, R. A., Ryley, M. D., & Temporal, J. (1982). A study of disc cutting in selected British rocks. International *Journal of Rock Mechanics and Mining Sciences & Geomechanics Abstracts*, 19(3), 107–121. https://doi.org/10.1016/0148-9062(82)91151-2

Tan, Q., Zhu, Z. H., Xia, Y. M., Xie, L. J., Sun, X. J., & Li, B. H. (2013). Numerical modelling of the TBM disc cutter's kinematic behaviour during its wear process and experimental verification. *Applied Mechanics and Materials*, 321–324, 51–56. https://doi.org/10.4028/www.scientific.net/AMM.321-324.51

Thyagarajan, M. V., & Rostami, J. (2024). Study of cutting forces acting on a disc cutter and impact of variable penetration measured by full-scale linear cutting tests. *International Journal of Rock Mechanics and Mining Sciences*, 175, 105675. https://doi.org/10.1016/j.ijrmms.2024.105675

Tu, Z., & Lu, Y. (2009). Evaluation of typical concrete material models used in hydro codes for high dynamic response numerical analyses. *International Journal of Impact Engineering*, 36(1), 132–146. https://doi.org/10.1016/j.ijimpeng.2007.12.010

Tulu, I. B. (2009). Modelling PDC cutter rock interaction (Master's thesis, West Virginia University). Graduate Theses, Dissertations, and Problem Reports. Statler College of Engineering and Mineral Resources, Department of Mining Engineering.

Wang, H., Wei, J., Yan, G., Zhao, H., & Xu, J. (2024). Research on TBM disc cutter wear prediction based on CSM model. In Lecture Notes in Mechanical Engineering (pp. 635-648). Springer. https://doi.org/10.1007/978-981-97-1876-4_48

Wang, K., Tan, Q., Xia, Y., Xu, Z. (2010). The Simulation Analysis of the TBM Disc Cutter Phase Angle. In: Liu, H., Ding, H., Xiong, Z., Zhu, X. (eds) Intelligent Robotics and Applications. ICIRA 2010. Lecture Notes in Computer Science(), vol 6424. Springer, Berlin, Heidelberg. https://doi.org/10.1007/978-3-642-16584-9_33

Wicaksana, Y., Jeong, H., & Jeon, S. (2021). Numerical analysis of rock cutting process induced by a pick cutter considering dynamic properties of rock at intermediate strain rate. *Bulletin of Engineering Geology and the Environment*, 80, 9049–9069. https://doi.org/10.1007/s10064-021-02471-4

Xiao, N., Zhou, X. P., & Gong, Q. M. (2017). The modelling of rock breakage process by TBM rolling cutters using 3D FEM-SPH coupled method. *Tunnelling and Underground Space Technology*, 61, 90-103. https://doi.org/10.1016/j.tust.2016.10.004

Xie, L. X., Lu, W. B., Zhang, Q. B., Jiang, Q. H., Chen, M., & Zhao, J. (2017). Analysis of damage mechanisms and optimisation of cut blasting design under high in-situ stresses. *Tunnelling and Underground Space Technology*, 66, 19-33. https://doi.org/10.1016/j.tust.2017.03.009

Xu, C., Zhu, Y., Song, D., Guo, X., Liu, X., Wang, E., & Lu, R. (2022). Comparison of DEM models with different elemental dimensions for TBM disc cutter rock fragmentation. *Sustainability*, 14(19), 12909. https://doi.org/10.3390/su141912909

Yu, B. (2005). Numerical simulation of continuous miner rock cutting process (Doctoral dissertation, West Virginia University). Statler College of Engineering and Mineral Resources, Department of Mining Engineering.

Zhang, R., Xiao, Y., Zhao, M., & Zhao, H. (2024). MatDEM-based study of disc cutter force model in open TBM tunnels: Incorporating installation radius and synergistic effects. *Underground Space*, 17, 188-208. https://doi.org/10.1016/j.undsp.2024.01.003

Zhou, G., Wang, X., Wang, D., Luo, M., Hao, Z., & Wu, W. (2023). Study on rock-breaking efficiency evaluation of TBM disc cutters based on Rostami prediction equations. *Frontiers in Earth Science*, 11, 1178127. https://doi.org/10.3389/feart.2023.1178127

SAŽETAK

Numerička simulacija i regresijska procjena sila na rotacijskim diskovima pri rezanju stijena TBM-om

U ovome radu predstavljen je računalni postupak za procjenu sila na reznim diskovima tijekom rotacijskoga rezanja pri radu strojeva za bušenje tunela (TBM). koji objedinjuje programski paket LS-DYNA s metodom zaglađenih čestičnih Galerkinovih funkcija (SPG) te materijalnim modelom Riedel–Hiermaier–Thoma (RHT). Provedeno je ukupno 58 numeričkih simulacija kako bi se ispitao utjecaj radijalnoga položaja ugradnje rezača, čvrstoće stijene, dodirne površine i razmaka između rezača na intenzitet sila. Rezultati pokazuju da normalne, kotrljajuće i bočne sile rastu s porastom tlačne čvrstoće stijene i povećanjem kontaktne površine, dok se smanjuju s povećanjem radijusa ugradnje rezača. Regresijskom analizom temeljenom na prirodnim logaritamskim transformacijama dobivene su jednadžbe za procjenu sila visoke točnosti (R^2 = 0,80 – 0,91). Za svaki prilagođeni parametar prikazana je standardna pogreška te interval pouzdanosti od 95 %, čime se osigurava transparentnost, ponovljivost i statistička utemeljenost rezultata.

Ključne riječi:
rezanje rotacijskim diskom, SPG, RHT, regresijska procjena sila rezača, regresijsko modeliranje

Author's contribution

Ebrahim Farrokh (Associate Professor): conceptualization, methodology, data analysis, writing, reviewing and editing. **Hamid Rokhy** (Research Engineer): methodology, numerical analysis, reviewing and editing. **Davood Lotfi** (R&D director): methodology, reviewing and editing.
All authors have read and agreed to the published version of the manuscript.